A V2X Integrated Positioning Methodology in Ultra-dense Networks

A V2X Integrated Positioning Methodology in Ultra-dense Networks

Qirui Liu, Rongke Liu, *Senior Member, IEEE,* Zijie Wang, Lincong Han, and John S. Thompson, *Fellow, IEEE*

***Abstract*—Intelligent transport systems demand the provision of a continuous high-accuracy positioning service. However, a vehicle positioning system typically has to operate in dense urban areas where conventional satellite-based positioning systems suffer severe performance degradation. 5G technology presents a new paradigm to provide ubiquitous connectivity, where the vehicle-to-everything (V2X) communication turns out to be highly conducive to enable both accurate positioning and the emerging Internet of Vehicles (IoV). Due to the high probability of line-of-sight (LoS) communication, as well as the diversity and number of reference stations, the application of ultra-dense networks (UDN) in the vehicle-to-infrastructure (V2I) subsystem is envisaged to complement the existing positioning technologies. Moreover, the cooperative determination of location information could be enhanced by the vehicle-to-vehicle (V2V) subsystem. In this article, we propose a V2X integrated positioning methodology in UDN, in which the V2I, V2V and Inertial Navigation Systems (INS) are unified for data fusion. This formulation is an iterative high-dimensional estimation problem, and an efficient multiple particle filter (MPF)-based method is proposed for solving it. In order to mitigate the non-line-of-sight (NLoS) impact and provide a relatively accurate input to the MPF, we introduce an advanced anchor selection method using the geometry-based *K*-Means clustering (GK) algorithm based on the characteristics of network densification. Numerical results demonstrate that utilizing the GK algorithm in the proposed integrated positioning system could achieve 18.7% performance gains in accuracy, as compared with a state-of-art approach.**

***Index Terms*—Vehicle to everything (V2X), Internet of Vehicles (IoV), vehicle positioning, multiple particle filter (MPF), ultra-dense networks (UDN), non-line-of-sight (NLoS).**

I. Introduction

A. Motivation

ROAD safety and efficient management of time and energy are the main driving forces of intelligent transport systems (ITS), where continuous high-accuracy positioning has generally been recognized as an enabling technology [1]. In the meantime, the perception system evaluates the road environment based on the location estimation and uploads to the control and planning systems, which will then pave the way for supporting various ITS applications, (e.g., lane change warning, collision avoidance, and intelligent traffic scheduling).

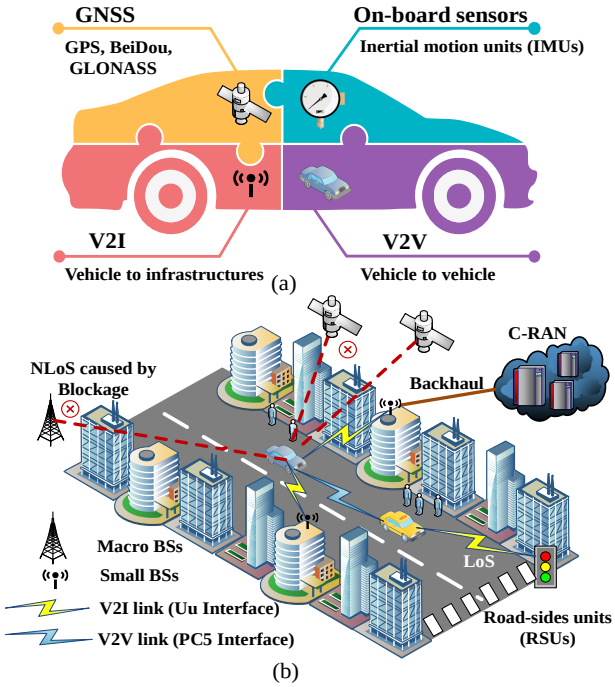

Fig. 1. Overview of positioning in the Internet of Vehicles: (a) typical positioning technologies; (b) main challenges in dense urban areas.

As shown in Fig. 1(a), existing vehicle positioning systems typically include a variety of technologies, such as the Global Navigation Satellite Systems (GNSS), on-board sensors and the terrestrial network-based positioning in Long Term Evolution (LTE) networks [2], [3]. However, a closer look into the existing technologies demonstrates their limitations from a vehicle positioning perspective. The GNSS-based technology offers a cheap and easily accessible absolute positioning solution, while satellite signals can easily be blocked or severely degraded in dense urban environments as shown in Fig. 1(b), leading to an inadequate accuracy ($\sim$ 10m) [3]. Although GNSS positioning accuracy could be improved through a real-time kinematic (RTK) technique, GNSS jammers and RTK cycle slips would inevitably lead to frequent system outages [4]. Radio access technology (RAT)-dependent positioning is in turn possible with the observed time difference of arrival (OTDoA) approaches in LTE networks, but it provides an accuracy of only a couple of tens of meters due to the limited coverage and signal blockage [5], which is unable to meet the

This work was supported by the Beijing Municipal Science and Technology Project (Z181100003218008). *(Corresponding author: Rongke Liu.)*

Q. Liu, R. Liu, Z. Wang and L. Han are with the School of Electronic and Information Engineering and Shenyuan Honors College, Beihang University, Beijing 100191, China (e-mail: {qirui_liu, rongke_liu, wangmajie, lincong_han}@buaa.edu.cn).

J. S. Thompson is with the Institute for Digital Communications, School of Engineering, University of Edinburgh, King's Buildings, Edinburgh, EH9 3JL, U.K. (e-mail: john.thompson@ed.ac.uk).

requirement of vehicular applications.

In order to complement the conventional vehicle positioning systems under these challenging conditions, a variety of inertial sensors such as accelerators and gyroscopes have been used to update the vehicle position relative to its previous estimate [3]. However, the main problem of the inertial sensors is unstable performance in terms of severe error accumulation caused by process noise. This problem can be reduced by correcting the estimated position frequently using other positioning systems like the GNSS, although cumulative errors can still be present ($\sim$ 7.2m) [6]. Researchers have shown the potential of fusing data from other high precision sensors to improve the accuracy and robustness, but at a relatively high cost [3].

Vehicle positioning typically depends on multifarious hardware and the corresponding techniques need to adapt to different conditions, and with different trade-offs. It should be noted that the terrestrial cellular radio infrastructure is easy accessible and would be further improved with the evolution into 5G and beyond. The importance of location-based services (LBS) was already highlighted in 3G networks, while dedicated positioning signals have only been established in 4G [7], by using the positioning reference signal (PRS) with specific pilot patterns.

Nowadays, the emerging Internet of things (IoT) technologies can provide vehicle-to-everything (V2X) connectivity [8], which supplements the existing dedicated short range communication (DSRC) standards based on IEEE 802.11p [9]. By exploiting the V2X communication channels, such as vehicle-to-vehicle (V2V) and vehicle-to-infrastructure (V2I), multiple information sources from internal and external environments could be fused to an integrated positioning system. This approach can use on-board sensors to further improve both accuracy and robustness at a relatively low cost. In particular, the ultra-dense networks (UDN), which is a vital property of future wireless communication systems [10], [11], would provide abundant reference stations, enabling an ubiquitous signal availability and a high probability of line-of-sight (LoS) transmission for accurate V2I measurements [12], [13]. We argue that V2X communications in UDN would complement existing positioning systems to provide high accuracy and redundancy for vehicular applications.

B. Related Work

With the proliferation of mobile devices and the growing demand for network services, ultra-dense networks comprising flexibly deployed base stations (BSs) is a promising solution to the explosive growth of network traffic [11]. Researches have shown that in UDN scenarios, the UEs are highly likely to have LoS propagation to one or more BSs at a time [12], [13]. Peral-Rosado *et al*. [14] have studied the positioning capabilities of future V2I networks in a highway scenario, where errors below 30 centimeters could possibly be achieved using a 100 MHz bandwidth signal in several ideal conditions. This research has revealed that 5G has the potential to utilize the existing infrastructure to provide positioning services at a limited additional cost, with accuracy higher than the GNSS [13]. However, these studies mainly focused on the LoS-dominated channel between UE and BSs, which is unrealistic since the LoS transmission in each link cannot always be guaranteed, and the signal bandwidth is usually limited. Although it is important to analyze the achievable performance of a positioning system under ideal cases, the performance under severe challenging conditions like the non-line-of-sight (NLoS) propagation in dense urban areas should also be investigated, which could help to design and provide a relatively safe and robust positioning service for the ITS applications [3]. Koivisto *et al*. [15] have studied the positioning in UDN where UEs transmit periodic uplink (UL) beacon signals and the networks estimate the directional and temporal parameters to carry out 3D positioning. This paper still assumed that LoS links could be accurately classified using received signal strength (RSS) features. Due to the fine time resolution afforded by ultra-wideband (UWB) signals, Venkatesh *et al*. [16] have designed a NLoS mitigation method based on linear programming, supposing that LoS and NLoS range estimates could be accurately distinguished. Besides the NLoS measurement errors, the poor geometry of anchors could increase the estimation errors of terrestrial network-based multilateration systems [17]–[19]. To find an optimal anchor set for ground UEs, Wang *et al*. [20] have proposed an efficient anchor selection method based on Horizontal Dilution of Precision (HDOP). Specifically, Zhang *et al*. [21] analyzed the optimal deployment strategies of road side units (RSU) evaluated by the Geometric Dilution of Precision (GDOP), where LoS conditions are still considered for all links. Thus, it is essential to study error mitigation methods considering both NLoS propagation effects and the undesirable geometric layout of anchors in UDN, which is one of the objectives of this article.

Generally speaking, a robust vehicle positioning system typically includes a variety of subsystems for data fusion [3]. In V2X networks, the V2I communication would provide absolute position information, while other techniques like the device-to-device (D2D) communications also provide direct, reliable links between vehicles. Research in [22] demonstrated the validity of positioning and tracking by adopting direction-of-arrival (DoA) and time-of-arrival (ToA) estimation in dense networks with the extended Kalman filter (EKF). However, cooperation between vehicles has been neglected in this study. Yin *et al*. [23] have proposed an integrated method using the GNSS and D2D communication, focusing on the efficient ranging protocol for D2D positioning. Elazab *et al*. [24] explored an integration scheme using the round trip time (RTT) and RSS techniques between vehicles with on-board inertial sensors in GNSS-denied environments. However, this paper only considered V2V measurements and V2I measurements were neglected. Up to now, the integration of V2X communication in UDN for vehicle positioning enhancement has not been fully studied.

C. Main Contributions

In this article, we propose a V2X integrated positioning methodology in UDN, in which the measurement information

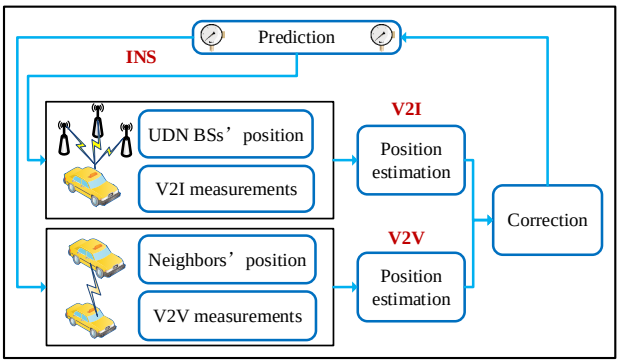

Fig. 2. The model of the proposed V2X integrated positioning.

from the V2I, V2V and INS subsystems is fused by the multiple particle filter (MPF) approach. To further mitigate the impact of NLoS propagation in dense urban areas, we develop a geometry-based K-Means clustering (GK) algorithm for the V2I subsystem to provide a relatively accurate input to the MPF. Specifically, the main contributions of this article are summarized as follows.

- In harsh environment like dense urban, signals can easily be blocked or severely degraded. To overcome these challenges, we propose a V2X integrated positioning system by exploiting the V2I, V2V and INS subsystems in future IoV. We demonstrate its potential for enabling continuous high-accuracy vehicle positioning.
- The posterior distribution of the proposed integrated positioning system is derived. In order to reduce the computational burden caused by the high-dimensional state space, we transform the original integration system into a distributed form, and a multiple particle filter (MPF)-based method is introduced.
- In order to provide a relatively accurate input to the MPF, we focus on the enhancement of the V2I subsystem. The main factors degrading the OTDoA positioning in cellular networks are analyzed theoretically when considering network densification.
- To alleviate the estimation error caused by poor anchor geometry and NLoS propagation effects, we propose a novel geometry-based K-Means clustering (GK) algorithm by exploiting the numerous BSs provided by UDN.

The rest of this paper is structured as follows. Section II introduces the system model, where three subsystems used for integrated positioning are introduced and analyzed. Section III derives the posterior distribution of UE's state under the integrated positioning system, which is constructed by the MPF approach. Section IV designs a GK-based V2I positioning enhancement method to eliminate the impact of NLoS propagation. Section V includes an analysis of the performance of our proposed methodology via simulations. Section VI concludes the paper.

II. System Model

In this article, as shown in Fig. 1(b), we consider a V2X scenario consisting of L stationary UEs, M moving UEs, and N terrestrial UDN BSs, which are densely deployed on both sides of the road. The moving UEs we considered are vehicles driving through an urban canyon within the V2V communication range, while the vehicles parked on the side of the roads or the pedestrians are modeled as stationary UEs. The BSs and two kinds of UEs are denoted by sets $\mathbb{N} \triangleq \{1, 2, \cdots, N\}$, $\mathbb{L} \triangleq \{1, 2, \cdots, L\}$ and $\mathbb{M} \triangleq \{1, 2, \cdots, M\}$, respectively. The 3D location of each BS is fixed and available to the UEs, which can be expressed as $\mathbf{b}^n = \left[\mathrm{b}_x^n, \mathrm{b}_y^n, \mathrm{b}_z^n\right]^T \in \mathbb{R}^{3\times 1}, n \in \mathbb{N}$, and the location of UE i is denoted as $\mathbf{I}^i = \left[\mathrm{I}_x^i, \mathrm{I}_y^i, \mathrm{I}_z^i\right]^T \in \mathbb{R}^{3\times 1}, i \in \{\mathbb{L}, \mathbb{M}\}$.

The integrated positioning model is shown in Fig. 2, where each UE obtains location information from three subsystems: 1) the V2I positioning subsystem; 2) the V2V positioning subsystem; and 3) the INS positioning subsystem. The V2I positioning subsystem is used to estimate the UE's absolute location through the downlink channel of BSs in UDN. The V2V positioning subsystem could also generate UE's absolute location estimate by utilizing the relative distance and angle measurements between vehicles. The INS positioning subsystem is used to predict the UE's state based on the previous estimate and readings from inertial sensors. The integration process of these subsystems includes the "prediction" and "correction" stages. As shown in Fig. 2, for a given previous estimate, the INS is firstly used for state prediction. Then, the V2I and V2V subsystems generate the corresponding absolute position estimates to correct the prediction results. In this section, the operating principle of these three subsystems and their potentials and challenges in vehicle positioning will be analyzed in detail.

A. Model of V2I Positioning Subsystem

The OTDoA is a RAT-dependent positioning solution that exists in the 4G standards and is considered as a promising candidate technology for 5G positioning [25]. In this study, the OTDoA technology is utilized in the V2I positioning subsystem, where the UE first measures the ToA of a positioning reference signal (PRS) transmitted by the BSs in the UDN. Then, the time-difference-of-arrival (TDoA) observations are extracted according to the master station, and a position estimation is generated based on the weighted least squares (WLS) algorithm [26]. As shown in Fig. 2, several BSs in the UDN are selected as anchors to locate a UE, and the BS with strongest signal is the master anchor. The signal-to-interference-plus-noise ratio (SINR) corresponding to BS n is given by

$$SINR_n = \frac{p_{t,n}/PL_n}{\sum\limits_{m\in\mathcal{J}_n, m\neq n} p_{t,m}/PL_m + p_{noise}} \tag{1}$$

where $p_{t,n}$ is the transmitting power of n-th BS; p_{noise} is the received noise power; $\mathcal{J}_n$ is the set of BSs that share the same time or frequency resources with BS n; PL_n is the pathloss according to the urban micro cell (UMi) channel model in street canyon scenario [27]. The LoS/NLoS status are related to both the pathloss and ToA estimation, which are critical for

the design of positioning system. The LoS probability in the above scenario given by [27] can be expressed as

$$p_{LoS}\left(d_{2\mathrm{D}}\right)=\begin{cases}1 & ,d_{2\mathrm{D}}\leqslant 18\mathrm{m}\\ \frac{18}{d_{2\mathrm{D}}}+\exp\left(-\frac{d_{2\mathrm{D}}}{36}\right)\left(1-\frac{18}{d_{2\mathrm{D}}}\right) & ,18\mathrm{m}<d_{2\mathrm{D}}\end{cases} \tag{2}$$

where $d_{2\mathrm{D}}$ is the 2D distance between the UE and BS. The decision of LoS/NLoS status is realized by a uniform random variable in the range $[0,1]$. If the realization is less than $p_{LoS}\left(d_{2\mathrm{D}}\right)$ in (2), the state is LoS; otherwise it is NLoS. Then, the set of anchors is defined as $\mathbb{N}'=\{n|\, n\in\mathbb{N}, SINR_n\geqslant\delta_{\mathrm{SINR}}\}$, in which the master anchor is labeled as 1, and the size of $\mathbb{N}'$ is N'. Denote c as the speed of light, the ToA measurement with anchor n can be expressed as

$$\hat{t}_n=\frac{d_n}{c}+\Delta\tau_n+e_n \tag{3}$$

where d_n and $\hat{t}_n$ is the 3D Euclidean distance and the corresponding ToA measurement between the UE and anchor n, while the clock offset error is $\Delta\tau_n$ and the measurement error e_n is caused by noise. Considering the excess delay caused by NLoS transmission, the NLoS status is modeled by adding a positive delay δ_{NLoS} on e_n. As analyzed in [28], based on the orthogonal frequency division multiplexing (OFDM) modulation, the variance of the ToA measurement is given by

$$\sigma^2_{\mathrm{ToA}}(\hat{t}_n)=\frac{T_s^2}{N_{\mathrm{sub}}\cdot 8\pi^2\cdot SINR_n\cdot\sum\limits_{s\in\mathcal{S}}\sum\limits_{q\in\mathcal{N}_c}p_q^2\cdot q^2} \tag{4}$$

where T_s is the symbol duration of the received OFDM signal; N_{sub} is the number of subframes; $\mathcal{S}$ is the subset of symbols containing the PRS signal within one subframe; $\mathcal{N}_c$ is the subset of subcarriers used to transmit the PRS; p_q^2 is the relative power weight of subcarrier q.

It is worth noting that new network architectures, especially the cloud radio access network (C-RAN) [29], [30], will make the implementation of precise positioning in UDN more convenient, where ideal muting and perfect network synchronization could be achieved. As a result, the positioning resources could be transmitted in a centralized coordinated way to avoid the interference such that the SINR in (1) can be considered equal to the signal-to-noise-ratio (SNR) [28] and $\Delta\tau_n=\Delta\tau,\forall n\in\mathbb{N}'$. Without loss of generality, the TDoA observation between anchor m and n ($m,n\in\mathbb{N}'$) can be expressed as

$$\Delta\hat{t}_{m,n}=\hat{t}_m-\hat{t}_n=\frac{1}{c}\cdot\left(\|\mathbf{I}-\mathbf{b}_m\|-\|\mathbf{I}-\mathbf{b}_n\|\right)+\left(e_m-e_n\right). \tag{5}$$

Hence, the measurement of relative distance is given by

$$\hat{d}_{m,n}=h_{m,n}\left(\mathbf{I}\right)+e_{m,n}=c\Delta t_{m,n}+e_{m,n} \tag{6}$$

where $c\Delta t_{m,n}$ is the real distance difference and $e_{m,n}$ represents the additive error. To estimate the UE's position, we use WLS method to minimize the given norm of the difference of observations and the measurement model [26]. Each iteration step of the WLS in matrix form is defined as

$$\hat{\mathbf{I}}_t=\hat{\mathbf{I}}_{t-1}+\left(\mathbf{H}^T\mathbf{W}^{-1}\mathbf{H}\right)^{-1}\mathbf{H}^T\mathbf{W}^{-1}\left(\hat{\mathbf{d}}-\mathbf{h}\left(\hat{\mathbf{I}}_{t-1}\right)\right) \tag{7}$$

where $\hat{\mathbf{I}}_{t-1}$ is the estimation result of step $t-1$; $\mathbf{W}=\mathrm{diag}(\sqrt{\left(1.1\times10^4\right)\cdot10^{-B\cdot SNR_n/10}})$ is the weighted matrix constructed by SNR values [31], and B is the bandwidth; $\mathbf{H}\left(\mathbf{I}\right)=\nabla\mathbf{h}\left(\mathbf{I}\right)$ is the Jacobian matrix of the relative distance equations, which can be expressed as

$$\mathbf{H}\left(\mathbf{I}\right)=\begin{bmatrix}\frac{\partial\mathbf{h}_{2,1}(\mathbf{I})}{\partial\mathrm{I}_x} & \frac{\partial\mathbf{h}_{2,1}(\mathbf{I})}{\partial\mathrm{I}_y} & \frac{\partial\mathbf{h}_{2,1}(\mathbf{I})}{\partial\mathrm{I}_z}\\ \vdots & \vdots & \vdots\\ \frac{\partial\mathbf{h}_{N',1}(\mathbf{I})}{\partial\mathrm{I}_x} & \frac{\partial\mathbf{h}_{N',1}(\mathbf{I})}{\partial\mathrm{I}_y} & \frac{\partial\mathbf{h}_{N',1}(\mathbf{I})}{\partial\mathrm{I}_z}\end{bmatrix} \tag{8}$$

and the expressions of $\left[\frac{\partial\mathbf{h}_{n,1}(\mathbf{I})}{\partial\mathrm{I}_x}\right]$, $\left[\frac{\partial\mathbf{h}_{n,1}(\mathbf{I})}{\partial\mathrm{I}_y}\right]$ and $\left[\frac{\partial\mathbf{h}_{n,1}(\mathbf{I})}{\partial\mathrm{I}_z}\right]$ are shown in [5]. Denote the update value $\delta\hat{\mathbf{I}}_{t-1}=\left(\mathbf{H}^T\mathbf{W}^{-1}\mathbf{H}\right)^{-1}\mathbf{H}^T\mathbf{W}^{-1}\left(\hat{\mathbf{d}}-\mathbf{h}\left(\hat{\mathbf{I}}_{t-1}\right)\right)$, the iteration in (7) is terminated when $\left\|\delta\hat{\mathbf{I}}_{t-1}\right\|\leqslant\delta_{\mathrm{WLS}}$ or iteration times $t=100$, and the output of the V2I subsystem is $\hat{\mathbf{I}}_t$.

B. Model of V2V Positioning Subsystem

In V2X networks, UEs could also communicate with other UEs except the BSs, thus forming a cooperative localization system, i.e., the V2V positioning system. Besides the time-based ranging techniques like the round trip time (RTT) [32], recent advances in massive antenna systems (massive MIMO) can provide additional degrees of freedom to enable more accurate vehicle location by exploiting angular information of radio channels [25], [33]. Thus, we assume that the UEs are equipped with high-end V2V transceivers to measure the relative distance and angle, and each UE to be localized can communicate with UEs within the V2V communication range $d_{\delta\mathrm{V}}$. The set of V2V neighbors of UE i at time k is denoted as $\mathcal{V}(i)=\left\{j|\, j\in\{\mathbb{L},\mathbb{M}\}, d_k^{(i,j)}\leqslant d_{\delta\mathrm{V}}\right\}$. The relative measurements between UE i and j ($j\in\mathcal{V}(i)$) include the Euclidean distance $d_k^{(i,j)}$, azimuth $\varphi_k^{(i,j)}$ and elevation $\theta_k^{(i,j)}$. In this research, we mainly focus on the adverse effect caused by the NLoS transmission in the V2I subsystem, while the measurements between vehicles are assumed as LoS-dominated and errors are modeled as $\mathbf{g}_k^{(i,j)}=[\varepsilon_{d,k}^{(i,j)},\varepsilon_{\varphi,k}^{(i,j)},\varepsilon_{\theta,k}^{(i,j)}]^T$ that follow the Gaussian distribution with zero mean and standard deviations $[\sigma_d^{\mathrm{V2V}},\sigma_\varphi^{\mathrm{V2V}},\sigma_\theta^{\mathrm{V2V}}]^T$. Then, the locations of UE i in both x, y, and z directions $\mathbf{I}_k^{(i)}=[\mathrm{I}_{k,x}^{(i)},\mathrm{I}_{k,y}^{(i)},\mathrm{I}_{k,z}^{(i)}]^T$ are obtained by

$$\begin{bmatrix}\mathrm{I}_{k,x}^{(i)}\\ \mathrm{I}_{k,y}^{(i)}\\ \mathrm{I}_{k,z}^{(i)}\end{bmatrix}=\begin{bmatrix}\mathrm{I}_{k,x}^{(j)}\\ \mathrm{I}_{k,y}^{(j)}\\ \mathrm{I}_{k,z}^{(j)}\end{bmatrix}-\begin{bmatrix}d_k^{(i,j)}\cos\left(\varphi_k^{(i,j)}\right)\cos\left(\theta_k^{(i,j)}\right)\\ d_k^{(i,j)}\sin\left(\varphi_k^{(i,j)}\right)\cos\left(\theta_k^{(i,j)}\right)\\ d_k^{(i,j)}\sin\left(\theta_k^{(i,j)}\right)\end{bmatrix}. \tag{9}$$

However, the above relative positioning process needs to be supported by the absolute location information $\mathbf{I}_k$. Accordingly, the V2V subsystem requires to be complemented by certain absolute positioning systems such as the V2I and the INS, which will be introduced as follows.

C. Model of INS Positioning Subsystem

In this study, we consider a low-cost Inertial Navigation System (INS) equipped on the moving UEs, which includes

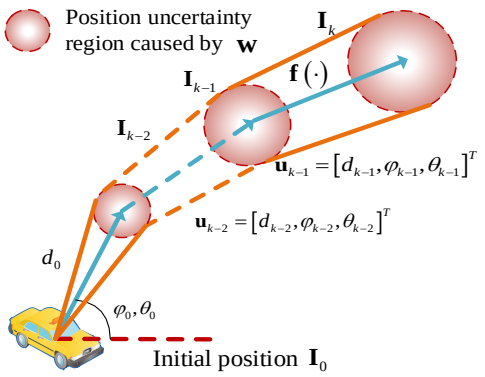

Fig. 3. The effect of error accumulation in the Inertial Navigation System (INS).

the odometer and gyroscope. The information from the sensors are transformed into the travel distance d, azimuth φ and the elevation θ, then the corresponding displacement is calculated [24]. To ensure the robustness of the whole system, errors are introduced to both the INS sensors and the UEs' initial positions $\|\tilde{\mathbf{I}}_0 - \mathbf{I}_0\|$. Starting from $\tilde{\mathbf{I}}_0$, the state transition function derived from the INS is given by

$$\mathbf{I}_k = \mathbf{f}\left(\mathbf{I}_{k-1}, \mathbf{u}_{k-1}, \mathbf{w}_{k-1}\right) \tag{10}$$

where $\mathbf{u}_{k-1} = [d_{k-1}, \varphi_{k-1}, \theta_{k-1}]^T$ is the information from sensors related to the UE's motion between time $k-1$ and k, and $\mathbf{w}_{k-1} = [\varepsilon^{\text{INS}}_{d,k-1}, \varepsilon^{\text{INS}}_{\varphi,k-1}, \varepsilon^{\text{INS}}_{\theta,k-1}]^T$ represents the process noise that is independent of the previous and present states, resulting from the inaccurate sensor readings.

However, as shown in Fig. 3, the performance of the commonly used Micro Electro Mechanical Systems (MEMS)-based inertial sensors degrades quickly as the vehicle travels, which results in severe error accumulation in the INS-based positioning [3]. Therefore, to avoid accumulated drift, the standalone INS needs to be corrected frequently by other systems such as the V2I and V2V analyzed in the above subsection.

III. V2X Integrated Positioning Method

As analyzed in Section II, the V2I, V2V and INS positioning subsystems could both help to generate certain location information. However, these systems also retain inherent drawbacks, such as signal blockage, error accumulation and inevitable dependence on absolute positioning. To overcome these weaknesses and enhance the system performance, these three subsystems are integrated as shown in Fig. 2, and the corresponding posterior distribution of the UE's state is derived in this section. Furthermore, we design a distributed architecture to reduce the original state dimension. Finally, the posterior distribution is constructed by the multiple particle filter (MPF) approach.

A. Posterior Distribution Function of the Proposed System

The errors and uncertainty in each subsystem, which in turn cause uncertainty in the estimation of UE's motion, motivate the use of a probabilistic approach for this state estimation problem. The state of the UE $\mathbf{I}_k^{(i)}$ is modeled as a vector of stochastic processes instead of a single-time best estimate. The aim of this approach is to estimate the probability density function of the UE's state at each integration time k conditioned on the whole measurement information until time k, i.e. the posterior distribution function (PDF). Besides, we assume that the 2-D location information of moving UEs is more critical to the network due to users' requirements. In a nutshell, the maximization of the posterior distribution of each moving UE's state is regarded as the objective function.

For a particular moving UE, the obtained information includes: 1) location estimates from the V2I subsystem at the ongoing integration time; 2) location information of its V2V neighbors approximated by the INS using the integrated positioning results at the previous integration time; and 3) V2V relative range and angle measurements at the ongoing integration time.

We denote $\mathcal{V}(i)$ as the set of V2V neighbors of UE i and $\mathcal{B}(i)$ as the set of selected BSs used for positioning, and $\mathcal{N}(i) = \{i, \mathcal{B}(i), \mathcal{V}(i)\}$. At each integration time k, the PDF of the UE's state $\mathbf{I}_k^{(i)}$ is generated according to the observations up to and including time k. Then, the state $\mathbf{I}_k^{(i)}$ which makes a maximum of the PDF is regarded as the integrated position estimation of UE, and can be expressed as

$$\hat{\mathbf{I}}_k^{(i)} = \arg\max_{\mathbf{I}_k^{(i)}} \text{post}\left(\mathbf{I}_k^{(i)}\right) = p\left(\mathbf{I}_k^{(i)} \middle| \mathcal{Z}_{1:k}^{(i,\mathcal{N}(i))}\right) \tag{11}$$

where $\text{post}\left(\mathbf{I}_k^{(i)}\right)$ can be expressed as (12) at the bottom of this page. $\mathcal{Z}_k^{(i,\mathcal{N}(i))} = [\mathcal{Z}_k^{(i,\mathcal{B}(i))}, \mathcal{Z}_k^{(i,\mathcal{V}(i))}, \mathbf{u}_{k-1}^{(i,\mathcal{V}(i))}]^T$ is information collected by UE i at integration time k, which includes the absolute position estimation $\mathcal{Z}_k^{(i,\mathcal{B}(i))}$ from the V2I subsystem according to (7), the angle and range measurements $\mathcal{Z}_k^{(i,\mathcal{V}(i))}$ with its V2V neighbors in $\mathcal{V}(i)$, and the IMU readings $\mathbf{u}_k^{(i)}$ from the INS.

For a given input $\text{post}\left(\mathbf{I}_{k-1}^{(i)}\right)$ from previous integration time $k-1$, the direct way to solve the problem P1 is to generate the joint PDF as shown in (12). Then, the PDF of a single UE is obtained through marginalization [23]. However, the unlimited increase of the number of V2V neighbors $\mathcal{V}(i)$ would inevitably lead to a high-dimensional state space $\mathbf{I}_k^{(i,\mathcal{V}(i))}$, which

$$\begin{aligned}\text{post}\left(\mathbf{I}_k^{(i)}\right) &= \int p\left(\mathbf{I}_k^{(i,\mathcal{V}(i))} \middle| \mathcal{Z}_{1:k}^{(\mathcal{N}(i))}\right) \partial\left(\mathbf{I}_k^{(\mathcal{V}(i))}\right) \\ &\propto \int \underbrace{p\left(\mathcal{Z}_k^{(i,\mathcal{V}(i))}, \mathcal{Z}_k^{(i,\mathcal{B}(i))}, \hat{\mathbf{I}}_{k-1}^{(\mathcal{V}(i))} \middle| \mathbf{I}_k^{(i,\mathcal{V}(i))}\right)}_{\text{State Correction - V2I \& V2V}} \underbrace{p\left(\mathbf{I}_k^{(i,\mathcal{V}(i))} \middle| \mathbf{I}_{k-1}^{(i,\mathcal{V}(i))}, \mathbf{u}_{k-1}^{(i,\mathcal{V}(i))}\right)}_{\text{State Prediction - INS}} \underbrace{\text{post}\left(\mathbf{I}_{k-1}^{(i,\mathcal{V}(i))}\right)}_{\text{Previous PDF}} \partial\left(\mathbf{I}_k^{(\mathcal{V}(i))}\right)\end{aligned} \tag{12}$$

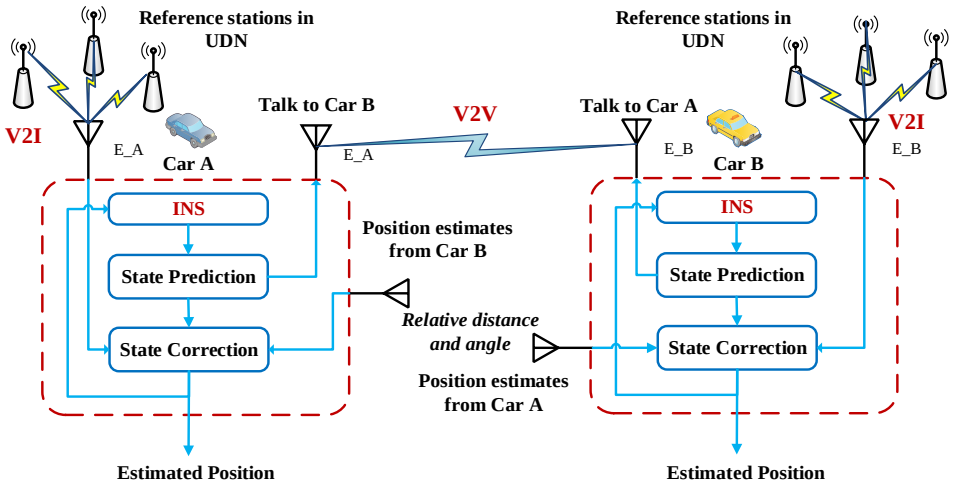

Fig. 4. Design of efficient V2X integrated positioning architecture in UDN.

is very difficult to solve optimally and inappropriate for the resource-constrained and delay-sensitive applications.

Thus, as shown in Fig. 4, we design an efficient integrated architecture to reduce the state dimension of the original problem. In the designed architecture, each UE only considers its own state and broadcasts the position estimation at the V2V measurement time. In this case, the original problem of calculating the PDF in (12) can be solved in a decentralized manner in each partitioned subspace $\mathbf{I}_k^{(i)}$ of the complete state space $\mathbf{I}_k^{(i,\mathcal{V}(i))}$.

Denote the output time of the V2I subsystem as k, and in order to facilitate the analysis of the integration process, we temporarily introduce an intermediate time $s \in [k-1, k]$. As analyzed in Section II-B, the V2V subsystem generates the location information of UE i by utilizing the relative measurements with UE j, $(j \in \mathcal{V}(i))$, and in particular, the absolute location information of UE j. Moreover, the measurement $\mathcal{Z}_s^{(j,\mathcal{B}(j))}$ and $\mathcal{Z}_s^{(i,j)}$ are independent. Thus, under the proposed integration architecture, the location information obtained by UE i at time s from the V2V subsystem can be expressed as

$$\begin{aligned}\mathrm{pv}\left(\mathbf{I}_s^{(i)}\right) = \int & p\left(\mathcal{Z}_s^{(j,\mathcal{B}(j))}\middle|\mathbf{I}_s^{(j)}\right) \\ & \cdot p\left(\mathcal{T}\left(\mathcal{Z}_s^{(i,j)}\right)\middle|\mathbf{I}_s^{(i)}, \mathbf{I}_s^{(j)}\right) \partial\left(\mathbf{I}_s^{(j)}\right)\end{aligned} \tag{13}$$

where $\mathcal{Z}_s^{(j,\mathcal{B}(j))}$ is the absolute position estimation from the V2I subsystem and $\mathcal{T}\left(\mathcal{Z}_s^{(i,j)}\right)$ represents the transformation of the V2V relative measurements to the vector from UE i to UE j, which can be written as

$$\mathcal{T}\left(\mathcal{Z}_s^{(i,j)}\right) = \mathbf{I}_s^{(j)} - \mathbf{I}_s^{(i)} = \begin{bmatrix} d_s^{(i,j)} \cos\left(\varphi_s^{(i,j)}\right) \\ d_s^{(i,j)} \sin\left(\varphi_s^{(i,j)}\right) \end{bmatrix} \tag{14}$$

where $\mathcal{Z}_s^{(i,j)} = [d_s^{(i,j)}, \varphi_s^{(i,j)}]^T$ is the distance and azimuth angle. However, the V2I output time is k, which means the absolute location information $\mathcal{Z}_s^{(j,\mathcal{B}(j))}$ is not available at time s. Therefore, $\mathcal{Z}_s^{(j,\mathcal{B}(j))}$ is approximated by $\mathcal{Z}_s^{(j,\mathcal{B}(j))} = \mathbf{f}\left(\hat{\mathbf{I}}_{k-1}^{(j)}, \mathbf{u}_{k-1}^{(j)}\right)$, in which $\mathbf{f}(\cdot)$ is the state transition function derived from the INS as shown in (10). Then, the PDF $\mathrm{post}\left(\mathbf{I}_k^{(i)}\right)$ in (12) can be simplified and is rexpressed as (15). It can be seen from the above analysis that the state dimension reduction has been achieved, but the corresponding positioning error of UE $j \in \mathcal{V}(i)$ is added into the estimation process. Furthermore, we set the position update time of the V2X integration system to be synchronized with the V2I subsystem, i.e., the intermediate time $s = k$, as shown in Fig. 4. Thus, the PDF $\mathrm{post}\left(\mathbf{I}_k^{(i)}\right)$ in

$$\begin{aligned}
&\mathrm{post}\left(\mathbf{I}_k^{(i)}\right) \propto \int p\left(\mathcal{Z}_k^{(i,\mathcal{B}(i))}, \mathcal{Z}_k^{(i,\mathcal{V}(i))}, \mathbf{f}\left(\hat{\mathbf{I}}_{k-1}^{(\mathcal{V}(i))}, \mathbf{u}_{k-1}^{(\mathcal{V}(i))}\right)\middle|\mathbf{I}_k^{(i,\mathcal{V}(i))}, \mathbf{u}_{k-1}^{(\mathcal{V}(i))}\right) \\
&\cdot p\left(\mathbf{I}_k^{(i,\mathcal{V}(i))}\middle|\mathbf{I}_{k-1}^{(i,\mathcal{V}(i))}, \mathbf{u}_{k-1}^{(i,\mathcal{V}(i))}\right) \partial\left(\mathbf{I}_k^{(\mathcal{V}(i))}\right) \mathrm{post}\left(\mathbf{I}_{k-1}^{(i,\mathcal{V}(i))}\right) \\
&\propto \int p\left(\mathcal{T}\left(\mathcal{Z}_s^{(i,j)}\right)\middle|\mathbf{I}_s^{(\mathcal{V}(i))}, \mathbf{I}_s^{(i)}\right) p\left(\mathbf{f}\left(\hat{\mathbf{I}}_{k-1}^{(\mathcal{V}(i))}, \mathbf{u}_{k-1}^{(\mathcal{V}(i))}\right)\middle|\mathbf{I}_s^{(\mathcal{V}(i))}, \mathbf{u}_{k-1}^{(\mathcal{V}(i))}\right) p\left(\mathbf{I}_s^{(i,\mathcal{V}(i))}\middle|\mathbf{I}_{k-1}^{(i,\mathcal{V}(i))}, \mathbf{u}_{k-1}^{(i,\mathcal{V}(i))}\right) \partial\left(\mathbf{I}_s^{(\mathcal{V}(i))}\right) \\
&\cdot p\left(\mathcal{Z}_k^{(i,\mathcal{B}(i))}\middle|\mathbf{I}_k^{(i)}\right) p\left(\mathbf{I}_k^{(i)}\middle|\mathbf{I}_s^{(i)}, \mathbf{u}_s^{(i)}\right) \mathrm{post}\left(\mathbf{I}_{k-1}^{(i,\mathcal{V}(i))}\right) \\
&\propto \underbrace{\mathrm{pv}\left(\mathbf{I}_s^{(i)}\right)}_{\text{V2V}} \cdot \underbrace{p\left(\mathcal{Z}_k^{(i,\mathcal{B}(i))}\middle|\mathbf{I}_k^{(i)}\right)}_{\text{V2I}} \underbrace{p\left(\mathbf{I}_k^{(i)}\middle|\mathbf{I}_s^{(i)}, \mathbf{u}_s^{(i)}\right) p\left(\mathbf{I}_s^{(i)}\middle|\mathbf{I}_{k-1}^{(i)}, \mathbf{u}_{k-1}^{(i)}\right)}_{\text{INS}} \underbrace{\mathrm{post}\left(\mathbf{I}_{k-1}^{(i,\mathcal{V}(i))}\right)}_{\text{Previous PDF}}
\end{aligned} \tag{15}$$

(15) is given by

$$\begin{aligned}\text{post}\left(\mathbf{I}_k^{(i)}\right) \;&\tilde{\propto}\; \text{pv}\left(\mathbf{I}_k^{(i)}\right)\\ &\cdot p\left(\mathcal{Z}_k^{(i,\mathcal{B}(i))}\middle|\mathbf{I}_k^{(i)}\right) p\left(\mathbf{I}_k^{(i)}\middle|\mathbf{I}_{k-1}^{(i)},\mathbf{u}_{k-1}^{(i)}\right)\text{post}\left(\mathbf{I}_{k-1}^{(i,\mathcal{V}(i))}\right)\end{aligned} \tag{16}$$

where the joint PDF in (12) does not need to be calculated, and the estimation in (11) under the proposed architecture is transformed into

$$\begin{aligned}\hat{\mathbf{I}}_k^{(i)} = \underset{\mathbf{I}_k^{(i)}}{\arg\max}\;\; &\text{pv}\left(\mathbf{I}_k^{(i)}\right) p\left(\mathcal{Z}_k^{(i,\mathcal{B}(i))}\middle|\mathbf{I}_k^{(i)}\right)\\ &\cdot p\left(\mathbf{I}_k^{(i)}\middle|\mathbf{I}_{k-1}^{(i)},\mathbf{u}_{k-1}^{(i)}\right)\text{post}\left(\mathbf{I}_{k-1}^{(i,\mathcal{V}(i))}\right).\end{aligned} \tag{17}$$

At integration time k, (17) can be considered as a data fusion process for UE i, where $\text{post}\left(\mathbf{I}_k^{(i)}\right)$ is the information from the V2V subsystem according to (15); $p\left(\mathcal{Z}_k^{(i,\mathcal{B}(i))}\middle|\mathbf{I}_k^{(i)}\right)$ is the location estimation from the V2I subsystem; $p\left(\mathbf{I}_k^{(i)}\middle|\mathbf{I}_{k-1}^{(i)},\mathbf{u}_{k-1}^{(i)}\right)$ is the state transition information of UE i from the INS to provide the continuity; and $\text{post}\left(\mathbf{I}_{k-1}^{(i,\mathcal{V}(i))}\right)$ is the prior information from the previous integration.

B. Multiple Particle Filter based Integrated Positioning Method

The integrated position estimation derived in (17) needs to be solved iteratively in the time domain to meet the continuity requirements of accurate vehicle positioning. In this subsection, we propose a multiple particle filter (MPF)-based method to solve the problem, in which the measurements generated from the V2I, V2V and INS subsystems are efficiently fused with relatively low computational burden.

Estimating the UE's states in a dynamical system is an instance of the Bayesian filtering problem, where the interest is in constructing the PDF through the integration stage of "Prediction" and "Correction" [34]. In traditional Bayesian filtering, the recursive use of Bayes theorem requires high complexity due to the multi-dimensional integrals. The commonly used Kalman filter (KF) and Extended KF-based integration algorithms, are generally implemented based on the assumption of a linearized system model. Another solution that avoids the linear assumption relies on approximating the multi-dimensional integrals numerically using the Sequential Monte Carlo method, which is the well-known particle filter (PF) [35]. This method samples from both the prior importance density and the observation likelihood, and propagates the PDF in the form of a set of weighted particles. However, the direct utilization of classical PF would inevitably lead to a high dimensional state space. To find an alternative method that would alleviate the explosion of necessary number of particles, the multiple PF (MPF) has recently been proposed [36], [37]. In the MPF, the complete state space is partitioned into subspaces and a separate particle filter is applied in each subspace, which is appropriate for solving (17).

Following the idea of the MPF, we assign a particle filter to each state vector $\mathbf{I}_k^{(i)}$. At time k, the PDF of UE i $p\left(\mathbf{I}_k^{(i)}\middle|\mathcal{Z}_{1:k}^{(i,\mathcal{N}(i))}\right)$ is represented by a set of random particles

Algorithm 1 Proposed MPF-Based Integrated Positioning Method

Input: Number of particles M_i, initial distribution $\text{post}\left(\mathbf{I}_0^{(i)}\right)$, likelihood calculation function $g(\cdot)$, maximal number of iteration time $k_{\max}$.
Output: Integrated position estimation $\hat{\mathbf{I}}_k^{(i)}$.
Initialization:
For particles $m = 1,\ldots,M_i$, generate the initial state according to $\text{post}\left(\mathbf{I}_0^{(i)}\right)$ and set the weight as $\pi_{i,k}^{(m)} = \frac{1}{M_i}$.
Repeat:
The prediction stage:
Sample the particles from previous iteration $\mathbb{S}_{i,k-1} = \left\{\left(\mathbf{I}_{i,k-1}^{(m)}, \pi_{i,k-1}^{(m)}\right)|m = 1,\ldots,M_i\right\}$ by $p\left(\mathbf{I}_{i,k}^{(m)}\middle|\mathbf{I}_{i,k-1}^{(m)},\mathbf{u}_{k-1}^{(i)}\right)$ from the INS;
The correction stage:
Generate the observations from V2I and V2V subsystem: $\mathcal{Z}_k^{(i,\mathcal{B}(i))}$, $\mathcal{Z}_k^{(i,\mathcal{V}(i))}$;
Calculate the weight according to the observation likelihood: $\pi_{i,k}^{(m)} = g\left(\text{pv}\left(\mathbf{I}_k^{(m)}\right) p\left(\mathcal{Z}_k^{(i,\mathcal{B}(i))}\middle|\mathbf{I}_k^{(m)}\right)\right)$;
Normalize the weights: $\tilde{\pi}_{i,k}^{(m)} = \pi_{i,k}^{(m)} / \sum_{m=1}^{M_i} \pi_{i,k}^{(m)}$, and the particle set becomes $\tilde{\mathbb{S}}_{i,k}$;
The resampling step:
Resample from $\tilde{\mathbb{S}}_{i,k} = \left\{\left(\tilde{\mathbf{I}}_{i,k}^{(m)}, \tilde{\pi}_{i,k}^{(m)}\right)|m = 1,\ldots,M_i\right\}$ such that $p\left(\mathbf{I}_{i,k}^{(m)} = \tilde{\mathbf{I}}_{i,k}^{(m')}\right) = \tilde{\pi}_{i,k}^{(m')}$;
For particles $m = 1,\ldots,M_i$, set $\pi_{i,k}^{(m)} = 1/M_i$;
Calculate the V2X integrated position estimation: $\mathbf{I}_k^{(i)} = (1/M_i)\sum_{m=1}^{M_i} \mathbf{I}_{i,k}^{(m)}$;
$k \leftarrow k+1$;
Until: $k = k_{\max}$.

$\mathbb{S}_{i,k} = \left\{s_{i,k}^{(1)},\ldots,s_{i,k}^{(M_i)}\right\}$, where M_i is the number of particles used by the i-th UE. The m-th particle is denoted as $s_{i,k}^{(m)} = \left\{\mathbf{I}_{i,k}^{(m)}, \pi_{i,k}^{(m)}\right\}$, where $\mathbf{I}_{i,k}^{(m)}$ is the value of the UE's state and $\pi_{i,k}^{(m)}$ is the corresponding weight. At time $k = 0$, the PF of UE i is initialized with the sample set $\mathbb{S}_{i,0} = \left\{s_{i,0}^{(1)},\ldots,s_{i,0}^{(M_i)}\right\}$ according to the initial distribution $\text{post}\left(\mathbf{I}_0^{(i)}\right)$ that encodes any information about the UE's initial state.

For the prediction stage of V2X integration, the particles are predicted according to $p\left(\mathbf{I}_{i,k}^{(m)}\middle|\mathbf{I}_{i,k-1}^{(m)},\mathbf{u}_{k-1}^{(i)}\right)$, which is fully specified by the state transition information and the corresponding noise in the INS subsystem. Then, in the correction stage, the V2I and V2V observations are used to adjust the weights of the particles, which can be calculated as

$$\pi_{i,k}^{(m)} = g\left(\text{pv}\left(\mathbf{I}_k^{(m)}\right) p\left(\mathcal{Z}_k^{(i,\mathcal{B}(i))}\middle|\mathbf{I}_k^{(m)}\right)\right) \tag{18}$$

where $g(\cdot)$ is the likelihood calculation function. If there is a short time outage caused by V2I or V2V, the INS measurements are used instead. Then, the particle set is resampled according to the section III in [38]. The obtained weighted particle set $\mathbb{S}_{i,k}$ approximates the probability density function in (17). The proposed MPF-based integration method is summarized in Algorithm 1.

IV. Enhanced V2I Positioning using the GK Algorithm

As analyzed in Section III-B, for a given set of V2X measurements, we can obtain its corresponding optimal estimation at this integration time by implementing Algorithm 1. However, in a harsh environment like dense urban, the inaccurate measurement of $\mathcal{Z}_k^{(i,\mathcal{B}(i))}$ caused by NLoS transmission would inevitably lead to an unsatisfactory filter result.

Considering a NLoS excess delay δ_{NLoS} that has not been detected in the measurement between UE and BS n in the V2I subsystem, the observation equations can be expressed as

$$\hat{\mathbf{d}}' = \mathbf{h}(\mathbf{I}) + \mathbf{e} + \boldsymbol{\mu}_n^T \delta_{\mathrm{NLoS}} \tag{19}$$

where $\boldsymbol{\mu}_n^T = [0, 0, \ldots, 1, 0, \ldots, 0]^T$ is the indicator of NLoS measurement and $\delta_{\mathrm{NLoS}} \geqslant 0$. According to (7), the corresponding parametric solution based on WLS estimation is given by

$$\hat{\mathbf{I}}' = \left(\mathbf{H}^T\mathbf{W}^{-1}\mathbf{H}\right)^{-1}\mathbf{H}^T\mathbf{W}^{-1}\hat{\mathbf{d}}'. \tag{20}$$

After modeling the bias $\boldsymbol{\mu}_n^T\delta_{\mathrm{NLoS}}$, the parametric solution is calculated as

$$\hat{\mathbf{I}} = \left(\mathbf{H}^T\mathbf{W}^{-1}\mathbf{H}\right)^{-1}\mathbf{H}^T\mathbf{W}^{-1}\left(\hat{\mathbf{d}}' - \boldsymbol{\mu}_n^T\delta_{\mathrm{NLoS}}\right) \tag{21}$$

and the estimation error caused by δ_{NLoS} is

$$\Delta\hat{\mathbf{I}} = \hat{\mathbf{I}}' - \hat{\mathbf{I}} = \left(\mathbf{H}^T\mathbf{W}^{-1}\mathbf{H}\right)^{-1}\mathbf{H}^T\mathbf{W}^{-1}\boldsymbol{\mu}_n^T\delta_{\mathrm{NLoS}}. \tag{22}$$

It can be seen from (22) that the undetected NLoS error would results in a biased estimation. To make matters worse, the poor geometry of anchors could further exacerbate the NLoS error, as the estimation error is also related to the Dilution of Precision (DOP) [39], which is given by

$$DOP = \sqrt{tr\left\{\left(\mathbf{H}^T\mathbf{H}\right)^{-1}\right\}}. \tag{23}$$

Note that we focus on the 2D positioning, we consider the Horizontal DOP (HDOP) in this article and the detailed expression is shown in [39], where a small HDOP implies a satisfactory geometric distribution. Thus, NLoS propagation of cellular signals and poor geometry of anchors are the two coupling factors leading to undesirable positioning performance of the V2I subsystem.

As shown in Fig. 5, we conducted a series of experiments to demonstrate the above analysis intuitively, in which 100 times of independent simulations are implemented for each case to show the effect of LoS/NLoS measurements, as well as the good/poor geometry of anchors. From Fig. 5(a) and Fig. 5(b), the HDOP values of the anchor set with good and poor geometry are 1.313 and 5.980, respectively, and the corresponding estimation results under LoS-dominated condition have revealed the significant influence of the geometry on accuracy. In this case, poor geometry of anchors may lead to unstable and divergent results when certain measurement errors are introduced. Fig. 5(c) shows an example, in which the NLoS error δ_{NLoS} has been directly incorporated into the WLS estimation, resulting in biased estimations (22). Finally, Fig. 5(d) has showed the poor geometry and NLoS error are two coupling factors, that is, a set of BSs with good geometry may contain large NLoS errors and vice versa, which could severely degrade the positioning accuracy.

Therefore, the NLoS and geometry factor should be considered comprehensively in the design of positioning enhancement techniques. Fortunately, the V2I subsystem enabled by UDN offers numerous reference stations with relatively high LoS probability, which provides the opportunities to select an appropriate anchor (i.e., BS) subset with satisfactory geometry and which are less affected by NLoS impact. In this section, by exploiting the BSs in UDN, we decouple the original BS selection problem into two sub-problems: 1) geometry-based BS selection; 2) NLoS error mitigation. These two sub-problems are solved sequentially by Algorithm 2 and 3, which are the first and second step of the proposed GK algorithm.

A. Geometry-based BS Selection

In order to optimize the geometry of BSs used for positioning, the direct way is to select the BSs subset with minimum HDOP, which can be expressed as the following combinatorial optimization problem:

$$\mathrm{P3}: \min_{\mathbf{s}\in\mathcal{S}} HDOP(\mathbf{s}, \mathbf{I}) \tag{24}$$

where $\mathbf{s}$ is a subset containing H ($H \geqslant 3$) BSs used for positioning; $\mathcal{S} = \{\mathbf{s}_1, \ldots, \mathbf{s}_J\}$ consists of all possible combinations of selecting H BSs out of N' BSs, where $J = \begin{pmatrix} N' \\ H \end{pmatrix}$; $HDOP(\cdot)$ is the function that calculates the HDOP value of a specific subset $\mathbf{s}$ according to [39]. Research [20] has proposed a BS selection method to select the BS subset with satisfactory geometry based on their azimuth and HDOPs, while the output is a single subset with minimal HDOP after the preliminary selection according to the azimuth. It is worth noting that a subset with good geometry may also contain a large NLoS error, leading to a biased estimation. Therefore, we modified the method in [20] by introducing a HDOP threshold δ_{HDOP} to retain subsets with satisfactory geometry, which are prepared for the NLoS error mitigation in the next step. The proposed geometry-based BS selection is summarized in Algorithm 2.

An application example is shown in Fig. 6, in which the parameters are set as $H = 6$, and interval angle of azimuth grouping $\Delta\varphi = 10°$. After the two step selection process in Algorithm 2, the number of BSs in group $1 \sim H$ are 3, 3, 2, 3, 3 and 3, respectively. Thus, the number of subsets in $\mathcal{S}^*$ is $J^* = \prod_{\eta=1}^{H} N'_\eta = 486$. It can be seen that the retained BS subsets by Algorithm 2 are approximately evenly distributed in azimuth, which is generally considered to be beneficial for position estimation [40]. Numerically speaking, the HDOP of each BS subset $\mathbf{s} \in \mathcal{S}^*$ does not exceed 1.3, which means that the geometry-based BS selection algorithm could effectively retain the BSs with a satisfactory geometry. In this case, the remaining factor degrading the system performance is the NLoS error, which will be discussed as follows.

B. NLoS Error Mitigation based on K-Means Clustering

As mentioned above, the retained subsets $\mathbf{s} \in \mathcal{S}^*$ are with good geometry as evaluated by the HDOP. If the system could

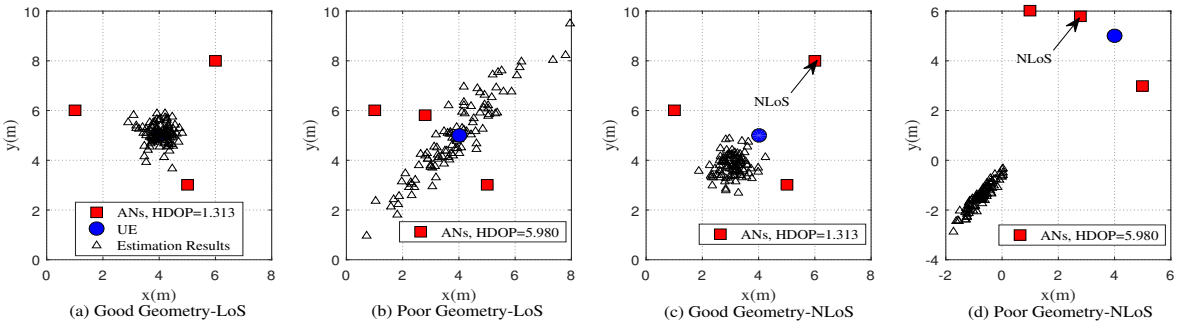

Fig. 5. Influence of good/poor geometry of anchor nodes (AN) and LoS/NLoS measurement on V2I positioning subsystem: (a) ANs are in good geometry and LoS-dominated, where the locations are $\mathbf{b}^1 = [1, 6]^T$, $\mathbf{b}^2 = [6, 8]^T$, $\mathbf{b}^3 = [5, 3]^T$. (b) ANs are in poor geometry and LoS-dominated, while $\mathbf{b}^2 = [2.8, 5.8]^T$. (c) ANs are in good geometry, but measurement with AN 2 contains NLoS error. (d) ANs are in poor geometry and the measurement with AN 2 contains NLoS error. In both cases, UE's position is $\mathbf{I} = [4, 5]^T$; the LoS measurement errors $e_n \sim \mathcal{N}(0, 0.1), \forall n \in \{1, 2, 3\}$, and the additional NLoS error $\delta_{\text{NLoS}} = 0.5$.

Algorithm 2 Geometry-based BS Selection Algorithm

Input: Number of BSs in a single subset H, interval angle of azimuth grouping $\Delta\varphi$, the set of available BSs in UDN $\mathbb{N}'$, approximated location of UE i at time k, i.e., $\tilde{\mathbf{I}}_k^i = \mathbf{f}(\hat{\mathbf{I}}_{k-1}^i, \mathbf{u}_{k-1}^i, \mathbf{w}_{k-1}^i)$, HDOP threshold δ_{HDOP}.

Output: The set consists of BS subsets with satisfactory geometry $\mathcal{S}^*$.

Preliminary Selection:

1: Compute the elevation $\theta_{i,n}$ and azimuth $\varphi_{i,n}$ between the approximated location of UE i and each BS n in $\mathbb{N}'$;

2: Select the BS n^* with the maximum elevation as the reference node for the preliminary grouping, i.e., $n^* = \arg\max_{n \in \mathbb{N}'} \theta_{i,n}$;

3: Set H grouping reference azimuths: $\varphi_\eta^{ref} = \varphi_{n^*} + \frac{2(\eta-1)}{H}\pi, \eta \in \{1, \ldots, H\}$;

4: Group the BSs according to the difference between the azimuth of each BS and the grouping reference azimuths φ_η^{ref}, i.e., BS n is assigned to group η if $|\varphi_{i,n} - \varphi_\eta^{ref}| \leqslant \Delta\varphi$;

5: If the number of BSs assigned to group η is zero, increase the value of $\Delta\varphi$ and regroup the BSs according to step (4) until there is at least one BS in each group, that is, group η includes N_η elements, $N_\eta \geqslant 1$;

Secondary Selection:

6: Select one BS from each group to form a subset, and the set of these BS subsets is formed as $\mathcal{S}_{pre} = \{\mathbf{s}_1, \ldots, \mathbf{s}_{J_{pre}}\}$, where $J_{pre} = \prod_{\eta=1}^{H} N_\eta$;

7: Compute the corresponding HDOP of each subset: $HDOP_{\mathbf{s}_j}, \mathbf{s}_j \in \mathcal{S}_{pre}$;

8: Retain the subsets with satisfactory geometry according to $HDOP_{\mathbf{s}_j} \leqslant \delta_{\text{HDOP}}, \mathbf{s}_j \in \mathcal{S}_{pre}$, and then the number of BSs in group η becomes N'_η. The remaining subsets formulate $\mathcal{S}^* = \{\mathbf{s}_1, \ldots, \mathbf{s}_{J^*}\}$, where $J^* = \prod_{\eta=1}^{H} N'_\eta$.

detect the LoS components in these subsets, there will be no biased estimation according to (22). However, the aforementioned case is only applicable when the time resolution of the signal is relatively high and the LoS components have not been blocked. In this study, we consider a more realistic case where

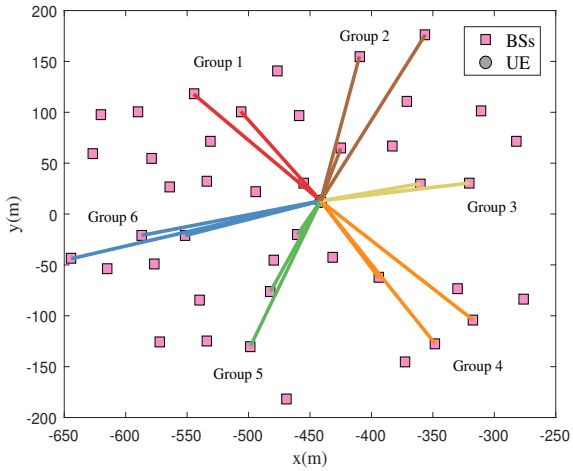

Fig. 6. Application example of the proposed geometry-based BS selection.

certain NLoS errors with unknown statistical information have contaminated the range measurements in the V2I subsystem and are not identifiable.

Letting $\mathbf{X} = \left\{\mathbf{x}_{\mathbf{s}_j} \middle| \mathbf{x}_{\mathbf{s}_j} \in \mathbb{R}^2, \mathbf{s}_j \in \mathcal{S}^*\right\}$ denote the WLS estimation results of each BS subset, the estimations less affected by the NLoS error are with certain consistency in $\mathbb{R}^2$ and relatively accurate according to (22), i.e., distributed closely to the true position. The results severely affected by the NLoS error, by contrast, are with lower aggregation degree in $\mathbb{R}^2$ caused by the uncertainty of NLoS errors. This analysis gives us an indication to utilize a novel data driven method for NLoS error mitigation. Considering the characteristics of the estimates that are more or less affected by NLoS error, we formulate a clustering problem in order to filter the solutions with higher degree of aggregation.

Accordingly, the K-Means is a classic clustering technique aiming to minimize the average Euclidean distance between data points in the same cluster [41], which is appropriate to solve the data driven-based NLoS error mitigation problem. Given an integer K and a set of data points $\mathbf{X} \in \mathbb{R}^2$, we utilize the K-Means++ algorithm [42], an improved method that is $o(\log k)$-competitive with the optimal clustering, to choose K centers $C = \{\mathbf{c}_1, \ldots, \mathbf{c}_K\}$ so as to minimize the potential

Algorithm 3 NLoS Error Mitigation based on K-Means Clustering

Input: Selected BS subsets with satisfactory geometry, i.e., the output $\mathcal{S}^*$ from Algorithm 2, number of clusters K.

Output: The BS subset $\mathbf{s}^*$ used for V2I positioning before the next anchor update period.

Initialization:

1: Compute the WLS estimation of each BS subset in $\mathcal{S}^*$ according to (7): $\mathbf{X} = \left\{\mathbf{x}_{\mathbf{s}_j} \middle| \mathbf{x}_{\mathbf{s}_j} \in \mathbb{R}^2, \mathbf{s}_j \in \mathcal{S}^*\right\}$;

NLoS error mitigation:

2: Select K cluster centers $C = \{\mathbf{c}_1, \ldots, \mathbf{c}_K\}$ to minimize the potential function $\phi(C;\mathbf{X}) = \sum_{\mathbf{x}_{\mathbf{s}_j} \in \mathbf{X}} \min \left\|\mathbf{x}_{\mathbf{s}_j} - \mathbf{c}_\kappa\right\|^2, \mathbf{c}_\kappa \in C$ according to the K-Means++ algorithm in [42];

3: Compute the number of data in each cluster: $\zeta_\kappa, \kappa \in \{1, \ldots, K\}$;

4: Select the cluster that includes the largest amount of data: $\kappa^* = \arg\max_{\kappa} \ \zeta_\kappa$;

5: Find the WLS estimation of a specific BS subset closest to $\mathbf{c}_{\kappa^*}$: $\mathbf{x}_{\mathbf{s}^*} = \arg\min_{\mathbf{x}_{\mathbf{s}_j} \in \mathbf{X}} \left\|\mathbf{x}_{\mathbf{s}_j} - \mathbf{c}_{\kappa^*}\right\|$;

6: Select the BS subset $\mathbf{s}^*$ as the anchor set of V2I positioning before the next anchor update period.

function:

$$\phi(C;\mathbf{X}) = \sum_{\mathbf{x}_{\mathbf{s}_j} \in \mathbf{X}} \min \left\|\mathbf{x}_{\mathbf{s}_j} - \mathbf{c}_\kappa\right\|^2 \tag{25}$$

where $\mathbf{c}_\kappa \in C$. Thus, the NLoS error mitigation method based on K-Means clustering is summarized in Algorithm 3.

An application example of the proposed NLoS error mitigation method is shown in Fig. 7, which is the next step after the example of geometry-based BS selection as shown in Fig. 6. The total number of estimation results corresponding to the BS subsets in $\mathcal{S}^*$ is $J^* = 486$, which are grouped into $K = 4$ clusters using the K-Means++ algorithm. The number of data in each cluster are 127, 108, 235, and 16, respectively. Cluster 1, 2 and 4 contain much less data as compared with cluster 3, which demonstrates the data in cluster 3 are with higher degree of aggregation, i.e., shorter average distance from the data points to the cluster center, and we assume the estimation results in cluster 3 are less affected by the NLoS impact, that is, $\kappa^* = 3$. The data point nearest to the κ^* cluster center $\mathbf{x}_{\mathbf{s}^*} = \arg\min_{\mathbf{x}_{\mathbf{s}_j} \in \mathbf{X}} \left\|\mathbf{x}_{\mathbf{s}_j} - \mathbf{c}_{\kappa^*}\right\|$ is selected as the final estimation, and the BS subset of $\mathbf{x}_{s^*}$, i.e., $\mathbf{s}^*$ will be the anchor set used for V2I positioning before the next anchor update period.

V. Simulation Results and Discussion

In this section, numerical simulation results are presented to evaluate the validity and performance of utilizing the proposed GK algorithm in the designed V2X integrated positioning system. First, we show the superiority of the proposed GK algorithm in the V2I subsystem, which is referred to below as the "GK-based method" for simplicity. Then, a series of Monte-Carlo simulations are conducted to prove that the proposed V2X integrated positioning method could bring a significant improvement in both accuracy and continuity, as compared with the non-integrated approach. In particular, with the relatively accurate input provided by the proposed GK-based method, the integrated positioning accuracy could be further improved. Finally, the influence of location uncertainty of stationary UEs and the number of particles in the MPF on the integration system are demonstrated.

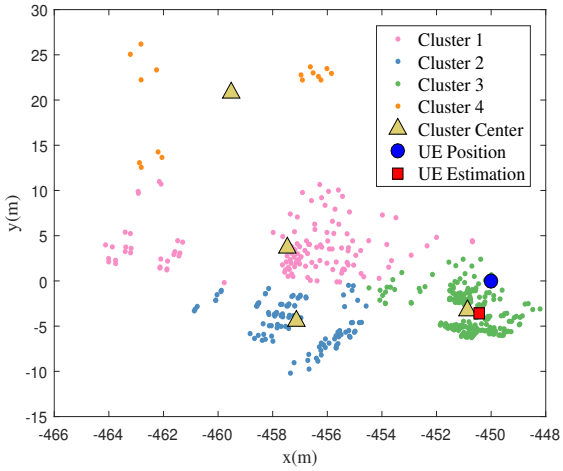

Fig. 7. Application example of the proposed NLoS error mitigation based on K-Means clustering.

Table I summarizes the key simulation parameters used in this section. Note that in the V2I subsystem, we assume the BSs which are more than 180 meters away from the UE will not be selected, since the probability of NLoS propagation is too large, and it will increase the computational cost of the proposed GK algorithm. As mentioned in Section II, we consider 2 moving UEs are driving along the positive direction of the x-axis in an urban canyon scenario. In each simulation, UE i and j start from $\mathbf{I}_0^i = [-450, 0]^T$, $\mathbf{I}_0^j = [-500, 0]^T$ with initial speed v_0 and uniformly accelerate to $v_{\max}$, and then the uniform linear motion is maintained until $k = k_{\max}$. Moreover, the stationary UEs are located at both sides of the roads with 100m spacing, which can be expressed as $[-525 + m \times 100, 15]^T, m \in \{1, \ldots, 10\}$ and $[-475 + (m-10) \times 100, -15]^T, m \in \{11, \ldots, 20\}$.

A. Evaluation of the Enhanced Non-integrated V2I Positioning

Before introducing the proposed GK-based V2I positioning method into the V2X integration system, we tested its effectiveness in the non-integrated V2I system. It should be noted that Fig. 6 and Fig. 7 are the application example for a single simulation run. In order to make the performance evaluation of the proposed GK-based method more statistically significant, 100 Monte-Carlo simulations are implemented. In this study, we compare the proposed GK-based method with 2 benchmark methods: 1) the most H powerful BSs out of N' are selected as the anchor set used for V2I positioning [5], which is referred to below as the "Max-SNR" method; 2) the BS subset with minimum HDOP generated from Algorithm 2 is utilized for position estimation [20], which is referred to below as the "Geometry-based" method.

TABLE I
SIMULATION PARAMETERS

Parameter	Value
Number of time slots ($k_{\max}$)	100
Length of time slots	1 s
Main frequency (f_c)	3.5 GHz
Signal bandwidth (B)	20 MHz
BS antenna pattern	Omni-directional
Symbol duration of the OFDM signal (T_s)	0.15 ms
Number of subframes (N_{sub})	4
Noise power density	−174 dBm/Hz
Total noise figure	9 dB
Interference modeling	Ideal muting
NLoS bias ($\delta_{\text{NLoS}} \geqslant 0$)[1]	$\sim \mathcal{N}\left(15, 8^2\right)$ m
Density of BSs (λ_{N})	318 BSs/km^2
Height of BSs (b_z^n)	15 m
BS layout on road sides	Uniform distribution
Minimum inter site distance (ISD)	30 m
Road width	40 m
Transmission power of BSs ($P_{\text{t,n}}$)	37 dBm
UE altitude (I_z)	1.5 m
Initial speed of the moving UE (v_0)	1 m/s
Acceleration of UE (a)	0.02×9.8 m/s^2
Maximum speed of UE ($v_{\max}$)	14.3 m/s
V2I anchor update period (T_{ap})	$10\text{m} \cdot speed^{-1}$ s
Initial position error of moving UEs	$\sim \mathcal{N}\left(0, 5^2\right)$ m
Location uncertainty of stationary UEs	$\sim \mathcal{N}\left(0, 5^2\right)$ m
Odometer error ($\varepsilon_d^{\text{INS}}$)	$\sim \mathcal{N}\left(0, (0.1 \times speed)^2\right)$
Gyroscope error ($\varepsilon_\varphi^{\text{INS}}$)	$\sim \mathcal{N}\left(0, 4^\circ/\sqrt{h}\right)$
Number of particles of each UE (M_i)	100
Likelihood calculation function ($g(\cdot)$)	$\|\cdot\|^{-2}$
V2I SNR threshold (δ_{SNR})	5 dB
V2V communication range ($d_{\delta\text{V}}$)	100 m
V2V distance measurement error (σ_d^{V2V})	$\sim \mathcal{N}(0, 1)$ m
V2V azimuth measurement error ($\sigma_\varphi^{\text{V2V}}$)	$\sim \mathcal{N}(0, 1)^\circ$
Number of BSs used for positioning (H)	6
Interval angle of azimuth grouping ($\Delta\varphi$)	10°
HDOP threshold (δ_{HDOP})	1.5
Number of clusters (K)	4

However, the Max-SNR method tries to select the powerful BSs with higher LoS probability, while the geometry of these BSs has been neglected. Similarly, the Geometry-based method focuses on the satisfactory geometry and does not consider the NLoS impact on estimation, making this method unsuitable in a harsh environment where signal blockage frequently occurs. Unlike these two methods, the proposed GK-based method designed for the V2I subsystem considers the coupling relationship of the anchor geometry and NLoS error, which are solved sequentially by the proposed Algorithm 2 and 3.

[1]In this paper, the standard deviation of the NLoS bias is set as a relatively large value to simulate the diverse and complex scenario in dense urban areas, which may be contrary to the assumption that $\delta_{\text{NLoS}} \geqslant 0$. For simplicity, we assume the simulated NLoS bias equals to zero if the realization of the random variable $\delta_{\text{NLoS}} < 0$.

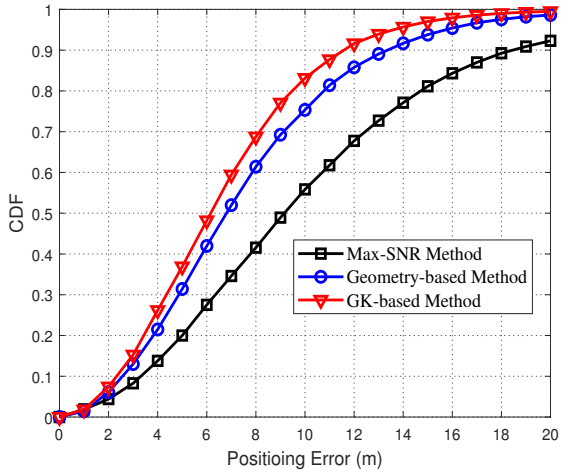

Fig. 8. Statistical evaluation corresponding to the three V2I positioning methods.

TABLE II
EVALUATION OF THE NON-INTEGRATED V2I POSITIONING

Method	50%	67%	80%	90%
Max-SNR	9.161	11.79	14.74	18.44
Geometry-based	6.805	8.702	10.74	13.38
GK-based	6.168	7.795	9.441	11.54

Fig. 8 shows the cumulative distribution functions (CDFs) of positioning errors in meter (m) of the aforementioned three V2I positioning method and the following percentiles are analyzed: 50%, 67%, 80%, 90%, as shown in Table II. It can be seen that the accuracy of the Max-SNR method degrades significantly due to the NLoS error and instability of geometry, while the Geometry-based method has optimized the distribution of anchors, thus reducing the median positioning error from 9.161 to 6.805 m, which means a 25.7% improvement in accuracy. Furthermore, the proposed GK-based method considers the NLoS error mitigation on the basis of satisfactory anchor geometry, which can improve the median accuracy by 32.7%. From the above statistical results, it can be concluded that the proposed GK-based method could significantly improve the accuracy of the non-integrated V2I positioning, which implies the potential to further enhance the performance of the V2X integration system. This will be analyzed in the next subsection.

B. Evaluation of the Proposed V2X Integrated Positioning

In this subsection, the validity and performance of the proposed V2X integrated positioning methodology (referred to below as the I-V2X for simplicity) are tested and evaluated via simulations, where the benchmark methods include the "non-integrated V2I (N-V2I)" and "integrated V2I (I-V2I)" positioning. The N-V2I represents the UEs only utilize the BSs for position estimation through V2I communication, while the I-V2I means that the UEs utilize the V2I and the INS subsystems to perform integrated positioning without V2V cooperation, i.e., $\hat{\mathbf{I}}_k^{(i)} = \arg\max_{\mathbf{I}_k^{(i)}} p\left(\mathcal{Z}_k^{(i,\mathcal{B}(i))} \middle| \mathbf{I}_k^{(i)}\right)$ ·

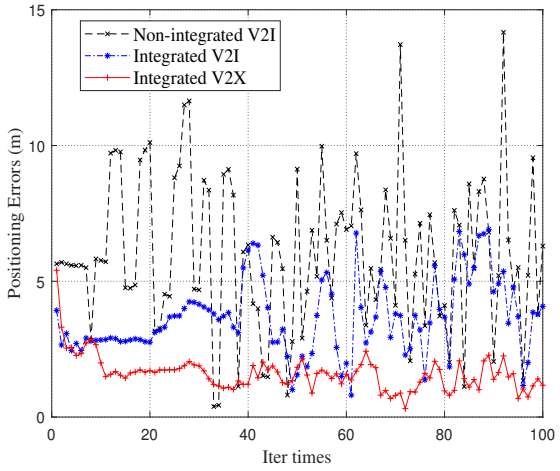

Fig. 9. Application example in a single time Monte-Carlo simulation. In all cases, the GK-based method is utilized in the V2I positioning.

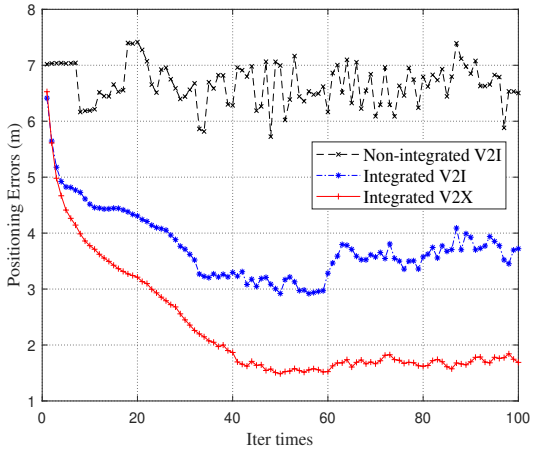

Fig. 10. Convergence behavior of positioning error with 100 times Monte-Carlo simulations. In all cases, the GK-based method is utilized in the V2I positioning.

$p\left(\mathbf{I}_k^{(i)}\middle|\mathbf{I}_{k-1}^{(i)},\mathbf{u}_{k-1}^{(i)}\right)$ post $\left(\mathbf{I}_{k-1}^{(i)}\right)$. In this study, we introduce a concept of "anchor update period" $T_{\text{ap}} = 10\text{m}\cdot speed^{-1}\text{s}$ for the V2I subsystem, since the frequent update of anchors in UDN is costly and unnecessary, especially when the UEs have a relatively low speed. To provide the spatial consistency in T_{ap}, the LoS/NLoS state shall be kept unchanged in each anchor update period. Note that in all V2X cases, we consider the average performance of the 2 moving UEs as evaluation metric, i.e., the positioning error at time k equals to $\left(\left\|\hat{\mathbf{I}}_k^i - \mathbf{I}_k^i\right\| + \left\|\hat{\mathbf{I}}_k^j - \mathbf{I}_k^j\right\|\right)/2$.

Fig. 9 shows a single time Monte-Carlo simulation of the I-V2X, I-V2I and N-V2I positioning, in which the proposed GK-based method is utilized in these cases. The performance of the N-V2I positioning tends to be fluctuate dramatically, because few information from other subsystems has been fused to provide the continuity under severe NLoS contamination. Intuitively, the I-V2I positioning performs much better than the non-integrated case, for the reason that the INS provides the state transition information to mitigate the tremendous errors from the V2I measurements. Moreover, when complemented by the V2V subsystem, the proposed I-V2X positioning outperforms the I-V2I case on both accuracy and continuity.

The statistical convergence behavior of these 3 cases are shown in Fig. 10, where 100 Monte-Carlo simulations are conducted for each case. As can be seen from the figure, the non-integrated positioning has a roughly constant error level since each estimation is independent, and the proposed MPF-based integrated positioning, i.e., the I-V2X and I-V2I, requires approximately 40 iterations to converge. Furthermore, compared with the I-V2I case, the proposed I-V2X case still offers a significant advantage in achieving higher positioning accuracy and better stability, because the information from the V2V subsystem (pv $\left(\mathbf{I}_k^{(i)}\right)$) as in (13) is exploited to mitigate the uncertainties in the V2I and INS subsystems. Although it seems that the positioning errors in this paper are of several meters and always above 1.5 meters, which is larger than the results in the related work [14], it should be noted that the simulation settings are based on a dense urban scenario with limited bandwidth and severe NLoS impact. However, the

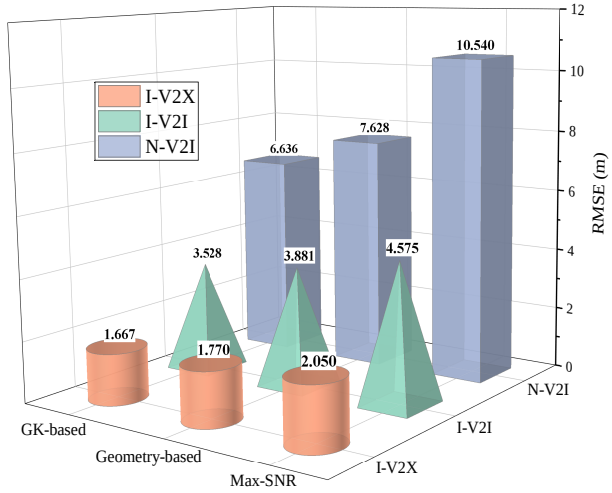

Fig. 11. Statistical comparison using the RMSE.

research in [14] mainly consider an achievable performance in highway scenario, where the assumptions include 100 MHz signal bandwidth and LoS-dominated channel. In general, the positioning error could possibly be further reduced by increasing the update frequency, allocating more wireless resources or equipping hardware with higher accuracy, etc.

As mentioned in the above subsection, for the V2I subsystem, we can utilize three positioning method, and the proposed GK-based method outperforms the others in terms of accuracy. In this subsection, we study the influence of different V2I positioning method on the integration system, that is, the influence of the input information $(p\left(\mathcal{Z}_k^{(i,\mathcal{B}(i))}\middle|\mathbf{I}_k^{(i)}\right))$ with different level of accuracy on the data fusion.

Fig. 11 shows the root mean square errors (RMSE) after convergence of the I-V2X, I-V2I and N-V2I positioning process, where each case has been tested with three V2I positioning methods. On the right part of Fig. 11, by utilizing the Max-SNR method, the RMSE of the proposed I-V2X is 55.2% lower than that of the I-V2I, and 80.6% lower than that of the N-V2I. These phenomenon and regularity remain

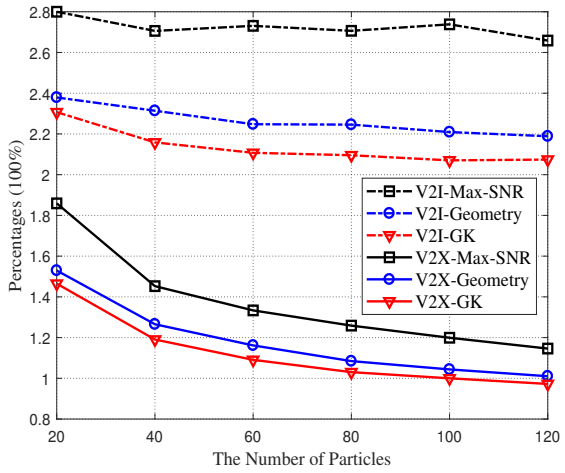

Fig. 12. Impact of the number of particles on the ratio of RMSE of the I-V2X and I-V2I positioning. The benchmark case is the proposed GK-based I-V2X positioning with 100 particles.

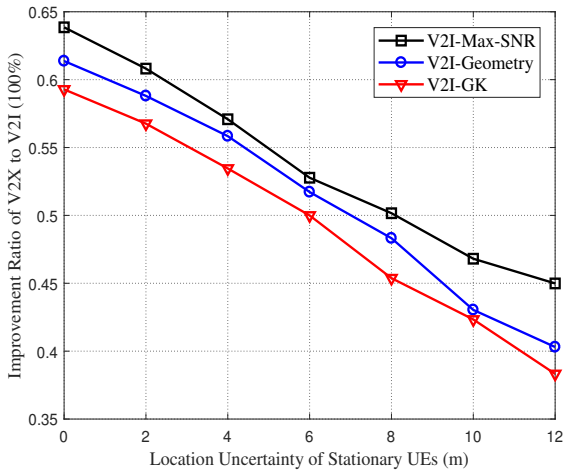

Fig. 13. Impact of location uncertainty of the stationary UEs on the improvement ratio of the proposed I-V2X relative to the I-V2I positioning, in which the standard deviation of the location errors is used as the evaluation metric for location uncertainty.

unchanged when analyzing the cases using the Geometry-based and the proposed GK-based methods. For a specific V2I method, the performance of the proposed I-V2X is generally better than that of the I-V2I, as well as the N-V2I. In particular, from Fig. 11, it can be observed that the RMSE of the I-V2X case also decreases when the V2I positioning method changes from the conventional Max-SNR to the proposed GK-based method, which could further reduces the RMSE by 18.7%. Accordingly, this conclusion also holds for the I-V2I and N-V2I cases. The proposed GK-based I-V2X positioning performs the best among those methodologies. This is expected since the proposed GK-based method could bring a relatively accurate input to the MPF as analyzed in Section V-A, where the NLoS and geometry factors are comprehensively considered to alleviate the estimation error $\left(\mathbf{H}^T\mathbf{W}^{-1}\mathbf{H}\right)^{-1}\mathbf{H}^T\mathbf{W}^{-1}\boldsymbol{\mu}_n^T\delta_{\text{NLoS}}$. Then, the MPFs are corrected with relatively accurate data from the V2I subsystem ($\mathcal{Z}_k^{(i,\mathcal{B}(i))}$) in the correction stage, i.e., the weights of the particles $\pi_{i,k}^{(m)} = g\left(\text{pv}\left(\mathbf{I}_k^{(m)}\right)p\left(\mathcal{Z}_k^{(i,\mathcal{B}(i))}\middle|\mathbf{I}_k^{(m)}\right)\right)$ are calculated more precisely, leading to a superior performance. Although the MPF could mitigate certain unstable errors through data fusion, the accuracy of the integration system is still in accordance with the quality of information from each subsystems.

In Fig. 12, the ratio of RMSE of the proposed I-V2X and I-V2I positioning is evaluated with the number of particles M_i utilized in each MPF (M_i varies from 20 to 120), where the benchmark case is the proposed GK-based I-V2X positioning with 100 particles. It is shown that for a specific method, the RMSE decreases when the number of the particles M_i grows. This is because a larger number of particles could search more potential locations in each prediction step, and then the particles closer to the UE's estimated position that derived from the V2I and V2V subsystems are given higher weights, which is beneficial to select and copy these particles in the resampling step. As M_i grows larger, the positioning accuracy continues to increase, but the rate of growth becomes slower, which is expected as the particles have almost covered the whole potential locations. The performance bottleneck is mainly caused by the inaccurate location information from the V2I and V2V subsystems used to calculate the likelihood function as in (18), i.e., the particles closer to the true position have not been given appropriate weights. On this occasion, the continuous increase of particles would result in high computational complexity, which is not merited, given the slight performance gains achieved. Therefore, the system should develop some novel data fusion method or to provide more accurate measurements for further improvements. Another observation from Fig. 12 is that for a particular V2I positioning method, the performance of the I-V2I is always worse than that of the proposed I-V2X and shows extremely limited gains as the number of particles increases. Similar to Fig. 10 and Fig. 11, Fig. 12 again demonstrates that fusing the V2V subsystem with the V2I and INS subsystems could significantly improve the I-V2X positioning performance.

In the above simulations, the proposed I-V2X generally outperforms the I-V2I positioning under the assumption that the location of the stationary UEs contains zero-mean Gaussian noises with 5 m standard deviation as shown in Table I. However, it is noteworthy that the location accuracy of the stationary UEs may vary in different situations, leading to uncertainty in the V2V cooperative determination of location information ($\text{pv}\left(\mathbf{I}_k^{(i)}\right)$), which may affect the performance of the integration system. Fig. 13 shows impact of the location uncertainty of the stationary UEs on the integration system, where the improvement ratio of the proposed I-V2X relative to the I-V2I positioning decreases as the degree of uncertainty increases. This phenomenon demonstrates that the V2V measurement error could spread to the V2X integration system, and thus cancel out the performance gains by introducing the V2V subsystem to the I-V2I positioning. Since the proposed I-V2X positioning could be affected by its data sources, it is necessary to detect the degree of uncertainty in each subsystem. For example, if the uncertainty of several V2V UEs is worse than a certain threshold, the data from the V2V subsystem

is no longer trustworthy, and the I-V2X should exclude these V2V cooperation to avoid performance degradation.

VI. Conclusion

In this article, we considered a V2X integrated system in UDN, where the V2I, V2V and INS subsystems are unified to provide continuous high-accuracy positioning service in dense urban areas. An efficient MPF-based method is proposed for data fusion, and to further mitigate the severe NLoS impact and provide a relatively accurate input to the MPF, we developed a GK algorithm for UDN, in which BS subsets with satisfactory geometry are firstly retained and the location estimation less affected by NLoS is then filtered by K-Means clustering. Numerical results demonstrate that the proposed V2X integrated positioning method achieves significant improvement over a non-integrated approach, and the proposed GK-based V2I positioning outperforms the Max-SNR method, which could further improve integration accuracy by 18.7%.

The results indicate that the deployment of UDN in dense urban areas is likely to make RAT-dependent positioning technologies very effective for accurate positioning of vehicles with limited cost. Future work is in progress to consider 1) NLoS error mitigation method in UDN based on stochastic geometry, and 2) fusing the GNSS and other positioning systems with practical measurements under the proposed V2X integration architecture.

References

[1] N. Lu, N. Cheng, N. Zhang, X. Shen, and J. W. Mark, "Connected vehicles: Solutions and challenges," *IEEE Internet of Things Journal*, vol. 1, no. 4, pp. 289–299, 2014.

[2] P. Misra and P. Enge, *Global Positioning System - signals, measurements and performance second edition*. Massachusetts: Ganga-Jamuna Press, 2006.

[3] S. Kuutti, S. Fallah, K. Katsaros, M. Dianati, F. Mccullough, and A. Mouzakitis, "A survey of the state-of-the-art localization techniques and their potentials for autonomous vehicle applications," *IEEE Internet of Things Journal*, vol. 5, no. 2, pp. 829–846, 2018.

[4] S. Stephenson, X. Meng, T. Moore, A. Baxendale, and T. Edwards, "Implementation of V2X with the integration of network RTK: Challenges and solutions," in *25th International Technical Meeting of the Satellite Division of the Institute of Navigation (ION GNSS 2012)*, Nashville, TN, 2012, pp. 1556-1567.

[5] H. Rydén, S. M. Razavi, F. Gunnarsson, S. M. Kim, M. Wang, Y. Blankenship, A. Grövlen, and A. Busin, "Baseline performance of LTE positioning in 3GPP 3D MIMO indoor user scenarios," in *2015 International Conference on Localization and GNSS (ICL-GNSS)*, 2015, pp. 1–6.

[6] F. Zhang, H. Stähle, G. Chen, C. C. C. Simon, C. Buckl, and A. Knoll, "A sensor fusion approach for localization with cumulative error elimination," in *2012 IEEE International Conference on Multisensor Fusion and Integration for Intelligent Systems (MFI)*, 2012, pp. 1–6.

[7] 3GPP TS 36.305, "Stage 2 functional specification of user equipment (UE) positioning in E-UTRAN, Std., Rel. 13," Dec. 2015.

[8] F. Yang, S. Wang, J. Li, Z. Liu, and Q. Sun, "An overview of Internet of Vehicles," *China Communications*, vol. 11, no. 10, pp. 1–15, 2014.

[9] L. Cheng, B. E. Henty, D. D. Stancil, F. Bai, and P. Mudalige, "Mobile vehicle-to-vehicle narrow-band channel measurement and characterization of the 5.9 GHz dedicated short range communication (DSRC) frequency band," *IEEE Journal on Selected Areas in Communications*, vol. 25, no. 8, pp. 1501–1516, 2007.

[10] H. Zhang, S. Huang, C. Jiang, K. Long, V. C. M. Leung, and H. V. Poor, "Energy efficient user association and power allocation in millimeter-wave-based ultra dense networks with energy harvesting base stations," *IEEE Journal on Selected Areas in Communications*, vol. 35, no. 9, pp. 1936–1947, 2017.

[11] N. Bhushan, J. Li, D. Malladi, R. Gilmore, D. Brenner, A. Damnjanovic, R. T. Sukhavasi, C. Patel, and S. Geirhofer, "Network densification: The dominant theme for wireless evolution into 5G," *IEEE Communications Magazine*, vol. 52, no. 2, pp. 82–89, 2014.

[12] Y. Liu, X. Shi, S. He, and Z. Shi, "Prospective positioning architecture and technologies in 5G networks," *IEEE Network*, vol. 31, no. 6, pp. 115–121, 2017.

[13] H. Wymeersch, G. Seco-Granados, G. Destino, D. Dardari, and F. Tufvesson, "5G mmwave positioning for vehicular networks," *IEEE Wireless Communications*, vol. 24, no. 6, pp. 80–86, 2017.

[14] J. A. del Peral-Rosado, J. A. López-Salcedo, Sunwoo Kim, and G. Seco-Granados, "Feasibility study of 5G-based localization for assisted driving," in *2016 International Conference on Localization and GNSS (ICL-GNSS)*, 2016, pp. 1–6.

[15] M. Koivisto, A. Hakkarainen, M. Costa, J. Talvitie, K. Heiska, K. Leppanen, and M. Valkama, "Continuous high-accuracy radio positioning of cars in ultra-dense 5G networks," in *2017 13th International Wireless Communications and Mobile Computing Conference (IWCMC)*, 2017, pp. 115–120.

[16] S. Venkatesh and R. M. Buehrer, "NLOS mitigation using linear programming in ultrawideband location-aware networks," *IEEE Transactions on Vehicular Technology*, vol. 56, no. 5, pp. 3182–3198, 2007.

[17] L. Cong and W. Zhuang, "Non-line-of-sight error mitigation in TDOA mobile location," in *2001 IEEE Global Telecommunications Conference (GLOBECOM)*, 2001, pp. 680–684.

[18] Q. Liu, R. Liu, Z. Wang, and Y. Zhang, "Simulation and analysis of device positioning in 5G ultra-dense network," in *2019 15th International Wireless Communications Mobile Computing Conference (IWCMC)*, 2019, pp. 1529–1533.

[19] Z. Deng, H. Wang, X. Zheng, and L. Yin, "Base station selection for hybrid TDOA/RTT/DOA positioning in mixed LOS/NLOS environment," *Sensors*, vol. 20, no. 15, pp. 4132–4149, 2020.

[20] Z. Wang, R. Liu, Q. Liu, J. S. Thompson, and M. Kadoch, "Energy-efficient data collection and device positioning in UAV-assisted IoT," *IEEE Internet of Things Journal*, vol. 7, no. 2, pp. 1122–1139, 2020.

[21] R. Zhang, F. Yan, W. Xia, S. Xing, Y. Wu, and L. Shen, "An optimal roadside unit placement method for VANET localization," in *2017 IEEE Global Communications Conference (GLOBECOM)*, 2017, pp. 1–6.

[22] M. Koivisto, A. Hakkarainen, M. Costa, P. Kela, K. Leppanen, and M. Valkama, "High-efficiency device positioning and location-aware communications in dense 5G networks," *IEEE Communications Magazine*, vol. 55, no. 8, pp. 188–195, 2017.

[23] L. Yin, Q. Ni, and Z. Deng, "A GNSS/5G integrated positioning methodology in D2D communication networks," *IEEE Journal on Selected Areas in Communications*, vol. 36, no. 2, pp. 351–362, 2018.

[24] M. Elazab, A. Noureldin, and H. S. Hassanein, "Integrated cooperative localization for connected vehicles in urban canyons," in *2015 IEEE Global Communications Conference (GLOBECOM)*, 2015, pp. 1–6.

[25] 3GPP TR 38.855, "Study on NR positioning support," v16.0.0, Mar. 2019.

[26] L. L. Scharf and C. Demeure, *Statistical signal processing: Detection, estimation, and time series analysis*. Addison-Wesley Reading, MA, 1991, vol. 63.

[27] 3GPP TR 38.901, "Study on channel model for frequencies from 0.5 to 100 GHz," v15.0.0, Jun. 2018.

[28] J. A. del Peral-Rosado, J. A. López-Salcedo, G. Seco-Granados, F. Zanier, and M. Crisci, "Achievable localization accuracy of the positioning reference signal of 3GPP LTE," in *2012 International Conference on Localization and GNSS (ICL-GNSS)*, 2012, pp. 1–6.

[29] C. Pan, M. Elkashlan, J. Wang, J. Yuan, and L. Hanzo, "User-centric C-RAN architecture for ultra-dense 5G networks: Challenges and methodologies," *IEEE Communications Magazine*, vol. 56, no. 6, pp. 14–20, 2018.

[30] H. Zhang, M. Feng, K. Long, G. K. Karagiannidis, and A. Nallanathan, "Artificial intelligence-based resource allocation in ultradense networks: Applying event-triggered Q-learning algorithms," *IEEE Vehicular Technology Magazine*, vol. 14, no. 4, pp. 56–63, 2019.

[31] L. Hsu, H. Tokura, N. Kubo, Y. Gu, and S. Kamijo, "Multiple faulty GNSS measurement exclusion based on consistency check in urban canyons," *IEEE Sensors Journal*, vol. 17, no. 6, pp. 1909–1917, 2017.

[32] H. Kloeden, D. Schwarz, E. M. Biebl, and R. H. Rasshofer, "Vehicle localization using cooperative RF-based landmarks," in *2011 IEEE Intelligent Vehicles Symposium (IV)*, 2011, pp. 387–392.

[33] A. Shahmansoori, G. E. Garcia, G. Destino, G. Seco-Granados, and H. Wymeersch, "5G position and orientation estimation through millimeter wave MIMO," in *2015 IEEE Globecom Workshops (GC Wkshps)*, 2015, pp. 1–6.

[34] J. Georgy, T. Karamat, U. Iqbal, and A. Noureldin, "Enhanced MEMS-IMU/odometer/GPS integration using mixture particle filter," *GPS Solutions*, vol. 15, no. 3, pp. 239–252, 2011.

[35] O. Hlinka, F. Hlawatsch, and P. M. Djuric, "Distributed particle filtering in agent networks: A survey, classification, and comparison," *IEEE Signal Processing Magazine*, vol. 30, no. 1, pp. 61–81, 2013.

[36] P. M. Djuric, T. Lu, and M. F. Bugallo, "Multiple particle filtering," in *2007 IEEE International Conference on Acoustics, Speech and Signal Processing - ICASSP '07*, vol. 3, 2007, pp. 1181–1184.

[37] P. M. Djurić and M. F. Bugallo, "Multiple particle filtering with improved efficiency and performance," in *2015 IEEE International Conference on Acoustics, Speech and Signal Processing (ICASSP)*, 2015, pp. 4110–4114.

[38] D. Arnaud, S. Godsill, and C. Andrieu, "On sequential monte carlo sampling methods for bayesian filtering," *Statistics and Computing*, pp. 197–208, 2000.

[39] J. A. Del Peral-Rosado, R. E. I Castillo, J. Miguez-Sanchez, M. Navarro-Gallardo, J. A. Garcia-Molina, J. A. López-Salcedo, G. Seco-Granados, F. Zanier, and M. Crisci, "Performance analysis of hybrid GNSS and LTE localization in urban scenarios," in *2016 8th ESA Workshop on Satellite Navigation Technologies and European Workshop on GNSS Signals and Signal Processing (NAVITEC)*, 2016, pp. 1–8.

[40] M. Zhang and J. Zhang, "A fast satellite selection algorithm: Beyond four satellites," *IEEE Journal of Selected Topics in Signal Processing*, vol. 3, no. 5, pp. 740–747, 2009.

[41] S. Lloyd, "Least squares quantization in PCM," *IEEE Transactions on Information Theory*, vol. 28, no. 2, pp. 129–137, 1982.

[42] D. Arthur and S. Vassilvitskii, "K-means++: The advantages of careful seeding," in *Proceedings of the Eighteenth Annual ACM-SIAM Symposium on Discrete Algorithms (SODA 2007)*, vol. 8, 2007, pp. 1027–1035.